Ultrashort Microwave-Induced Thermoacoustic Imaging: A Breakthrough in Excitation Efficiency and Spatial Resolution

Cunguang Lou, Sihua Yang, Zhong Ji, Qun Chen, and Da Xing*

MOE Key Laboratory of Laser Life Science and Institute of Laser Life Science, College of Biophotonics, South China Normal University, Guangzhou 510631, China

(Received 6 April 2012; published 20 November 2012)

With theoretical prediction and experimental validation, we propose a novel approach to significantly enhance the conversion efficiency of thermoacoustic (TA) imaging by using an ultrashort microwave pulse. The implementation of the ultrashort microwave pulse leads to orders of magnitude enhancement in excitation efficiency and spatial resolution, compared to that from existing TA imaging techniques. This allows high-resolution ($\sim$ 100 micron resolution) TA imaging to be acquired noninvasively. The present work represents a major breakthrough in the conversion efficiency of the TA effect and the resolution of TA imaging, which can potentially be used for clinical imaging.

DOI: 10.1103/PhysRevLett.109.218101 PACS numbers: 87.57.−s, 87.63.lm, 87.63.lt

Recently, there has been increasing interest in using the thermoacoustic (TA) effect for biomedical applications [1–5]. TA imaging takes advantage of the excellent resolution of ultrasound imaging while keeping the merit of high contrast and good tissue penetration of microwave [5–7]. The TA signal strength is proportional to the microwave energy density and microwave-to-acoustic conversion efficiency. Further enhancement of the conversion efficiency is critical for noninvasive imaging. Extensive efforts have been made to improve the efficiency of TA conversion by using exogenous contrast agents [8,9]; a significant improvement is yet to be achieved.

TA employs long-wavelength microwave pulse for the thermoelastic excitation, and thus yields a relatively deeper penetration [3,5,7], compared to that of laser-induced photoacoustic (PA) imaging [10–14]. The previously reported TA images were obtained via high-energy microwave pulse radiation, with a spatial resolution on the submillimeter level [1,2,15]. Although TA imaging exhibits an excellent performance in penetration depth, the relatively poor spatial resolution and potential risk of thermal damage to normal tissue limit its implementation in clinical settings.

Here we propose a novel approach to realize high-efficiency and high-resolution TA imaging and present the design of ultrashort microwave pulse (USMP) generator that is capable of generating high-peak-power nanosecond microwave pulse. Our method is based on a theoretical prediction that the excitation pulse duration is a crucial factor for the effective generation of ultrasonic waves. Compared with sub-microsecond microwave pulse, theoretical analysis shows that the employment of USMP leads to substantial enhancement in TA conversion efficiency and spatial resolution. The effect of the pulse duration on the TA signal was validated using micro- and nanosecond microwave pulses. The presented powerful and practical method opens up new opportunities for the application of TA in biomedical imaging.

In the thermoelastic regime the thermoacoustic pulse waveform will be determined by both the microwave absorption as well as the pulse duration [14]. Irradiation of the absorbing layer with a microwave pulse will result in an instantaneous heat deposition inside this layer and excites TA waves [3–5,10]. As in the case of linear acoustic system [16,17], the equation of thermoelastic sound excitation in a heat-conducting medium can be given as

$$\frac{\partial^2 \phi}{\partial^2 t} - {c_0}^2 \Delta \phi = \left(\frac{\beta {c_0}^2}{\rho_0 C_p}\right) \mathrm{div} S, \tag{1}$$

where $\phi(t, z)$ is the scalar potential of the velocity field, c_0 is the speed of sound, ρ_0 is the equilibrium density, C_p is the constant pressure heat capacity per unit mass and β is the coefficient of thermal expansion, ρ_0 is the equilibrium density, and S is the Poynting vector of the incident wave (the radiation intensity in the medium). For simplicity, we consider the one-dimensional problem. Assume a thin layer (10 μm) in homogeneous medium is illuminated by a relatively long microwave pulse ($\mu_a c_0 \tau_m \gg 1$) with a pulse duration of τ_m. Then the Poynting vector of the medium will be determined by $S = I_0 e^{-\mu_\alpha z} f(t) n_z$, where I_0 is the microwave intensity at the surface of the sample, μ_α is the absorption coefficient, z is the depth, n_z is the unit vector on the z axis and $f(t)$ describes the time dependence of microwave pulse [18]. Then the TA excitation can be described by

$$\frac{\partial^2 \phi}{\partial^2 t} - {c_0}^2 \frac{\partial^2 \phi}{\partial^2 z} = -\left(\frac{\mu_a {c_0}^2 \beta}{\rho_0 C_p}\right) I_0 e^{-\mu_a z} f(t). \tag{2}$$

With a Fourier transform on each side of the equation, ϕ can be solved using spectral method, and the vibration velocity (ν) of the particles can be obtained as $\nu = \mathrm{grad}\phi$. Consequently, the Gaussian microwave pulse

excited TA-signal profiles in the case of biological tissue imaging can be described by [17,18]

$$P(\tau, t) = -\frac{\mu_a I_0 \beta {c_0}^2}{2C_p} \int_{-\infty}^{\infty} f(t) e^{-\mu_a c_0 |\tau - t|} \mathrm{sgn}(\tau - t) dt. \quad (3)$$

According to the expression, the TA signal is consist of an exponential and inverse exponential form, the magnitude of TA pressure is directly related to the pulse energy, and the temporal profile relates to pulse duration. To validate the previous analytical results, we numerically simulated the TA waveforms as a function of pulse duration and the simulation results were depicted in Fig. 1. The pulse duration used in the simulation was varied from 450 ns to 10 ns and the corresponding value of $\mu_a c_0 \tau_m$ was within the range of 67.5 to 1.5.

Figure 1(a) provides temporal profiles of TA signals excited by Gaussian microwave pulse with various pulse durations and identical per pulse energy. The results show that the amplitude of TA signals increases with a decreasing pulse duration. This indicates an improvement in TA conversion efficiency. The time intervals between the two poles of TA signal are depicted in Fig. 1(b). Reducing microwave pulse width leads to a significant decrease in the time interval. When the microwave pulse duration decreased from 450 to 10 ns, the time interval between the two poles of TA signal decreased from 650 to 26 arbitrary unit (a.u.). It has been shown that TA imaging resolution is linearly related to the duration of the exciting TA waves, and shorter acoustic pulse provides higher resolution [9,17]. Thus, a 25-fold reduction in the acoustic signal width as a result of reducing microwave pulse width should lead to a 25-time higher spatial resolution.

In Fig. 1(c), the temporal profile of TA signals excited by microwave with identical peak power are plotted as a function of pulse duration, and the data extracted from the figure are displayed in Fig. 1(d). As shown in Fig. 1(c), the TA amplitude is seen to increases as the pulse duration increases. The solid line in Fig. 1(d) shows the dependence of microwave energy per pulse on pulse duration and the dots represents amplitude of TA signals. Given identical peak power, the energy per pulse linearly depends on the pulse duration. When the pulse duration increases from 10 to 200 ns, the microwave energy increase approximately 20 times. The increment of TA signal amplitude is estimated to 6 times, much less than the former, indicating that the TA conversion efficiency decreases with pulse duration increase.

The setup developed for experimental validation is schematically shown in Fig. 2(a). Pulsed microwave is used to illuminate the sample to excite TA waves that are subsequently captured by an ultrasound transducer and collected by a computer for data analyses. The core of the system is an USMP generator (Fig. S1 in the Supplemental Material [19]) that is based on high-voltage-pulsed power technology [20,21]. The USMP generator makes use of a charging circuit and Tesla transformer to produce a high-voltage pulse, and then discharge to the antenna for radiating microwave. The USMP generator has features of short pulse width, high peak power, simple structure, and easy miniaturization. The pulse duration is measured to be 10 ns with 800 ps rise time, the pulse repetition frequencies are

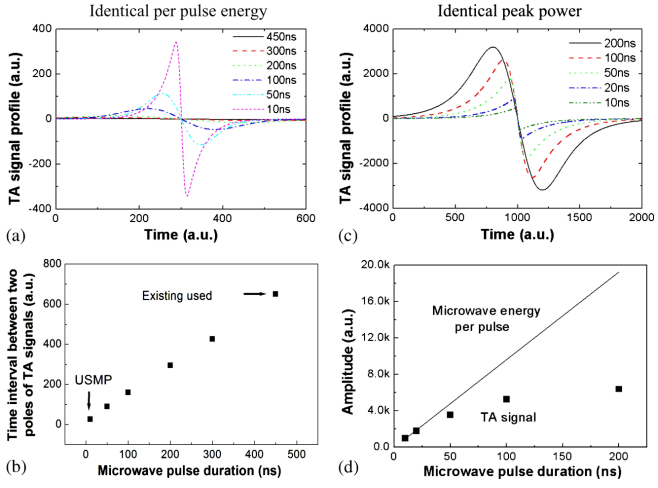

FIG. 1 (color online). Simulated TA waveforms versus microwave pulse durations. (a) TA waveform with various pulse duration and identical energy per pulse. (b) Time interval between two poles of the TA signal as a function of pulse duration. (c) TA waveform with various pulse duration and identical peak power. (d) The amplitude of the TA signal versus pulse duration for identical peak power; the solid line represents the microwave energy per pulse.

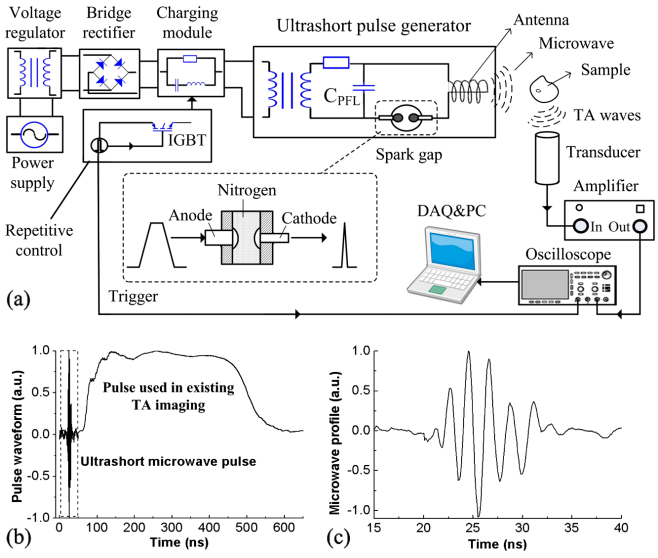

FIG. 2 (color online). (a) Schematic diagram of the experimental setup. (b) The comparison of the USMP and microwave pulse used in the existing TA imaging. (c) The temporal profiles of the USMP.

typically in the range of 1–100 Hz, and the peak output power is tunable from 2 to 40 MW.

In order to obtain high peak power and sharp front edges of microwave pulse, a spark gap was used and nitrogen at high pressure was pressed into the chamber of the spark gap to increase breakdown voltage. The breakdown voltage can be regulated by changing the gas pressure. That is, the output power of the pulse generator could be adjusted by tuning the gas pressure. The pulse duration of the microwave depends on the capacitor (C_{PFL}) of the resonant circuit whose capacitance value can be adjusted by changing the length of the PFL. Together with the spark gap, the PFL can produce short high-voltage pulses of several ns duration and deliver them to the antenna.

The antenna is another critical component of the USMP generator to radiate the fast transient electric fields. A helical antenna with a central frequency of 434 MHz was designed to convert the high-voltage short pulse to microwave radiation (Fig. S2 and Fig. S3 in Ref. [19]). In order to prevent dielectric breakdown and electric shock, the antenna was covered by an insulating layer of polypropylene material, and sulfur hexafluoride (SF_6) was pressed into the chamber of the antenna. In the near field region, the energy density around antenna is almost homogeneous distribution and is calculated to be adjustable between 15 and 360 $\mu\mathrm{J/cm}^2$.

The comparison of USMP and microwave pulse generally used in the existing TA imaging is shown in Fig. 2(b). The microwave pulse width used in our previous paper is 450 ns with 100 ns rise time [15]. The temporal profile of the USMP, as illustrated in Fig. 2(c), has a pulse duration of 10 ns and rise time of 800 ps. The USMP generator dramatically decreases the pulse duration with approximately two orders of magnitude.

In the data acquisition system, a focused ultrasonic transducer (I10P6NF20, DOPPLER, China) with a central frequency of 10 MHz (100% bandwidth at -6 dB), a focal length of 20 mm, and an active element of 6 mm in diameter was employed to detect the TA signals. To cover a 2π-receiving angle for TA imaging, a personal computer controlled the stepper motor to drive the sample rotating at 1.8°/step (Fig. S4) [19]. The acoustic pulse captured by the transducer was first amplified through a self-made wide bandwidth amplifier with a RC high-pass filter, then averaged 128 times by a digital oscilloscope (TDS3032B, Tektronix, USA) at a sampling rate of 500-M samples/s, and finally transferred to a personal computer for subsequent image processing. A modified filtered back-projection algorithm [7,22] was used to reconstruct the microwave absorption of objects from the measured data. The third derivative of the Gaussian wavelet was used to enhance sharpness of the boundaries.

Three series of experiments were conducted to verify the performance of the USMP-induced TA imaging: first, we compared the TA excitation efficiency at different microwave pulse durations; cross sections of two copper wires were subsequently imaged to verify the spatial resolution; then, a ring-shaped phantom was imaged and compared with the existing TA imaging. Phantoms made of 5% gelatin, 95% water were used in throughout the experiment. Finally, high-resolution TA images of copper wire targets with different shapes were reconstructed.

The TA conversion efficiency was compared for short- and long-pulse excitation. Fig. 3(a) gives the simulation results of the amplitude of the TA signal that shows in Fig. 1(a), which was excited by various microwave pulse durations with identical pulse energy. The fall-off in amplitude with increasing pulse duration is clearly in evidence. The temporal profiles of the captured TA signals from the phantom are displayed in Fig. 3(b), in which the longitudinal axis has been calibrated against the absorption coefficient, energy density per pulse, and the frequency response characteristic of the transducer. Experimental results show that the amplitude of the TA signal obtained by using a 10 ns microwave is 86-fold greater than that generated by a microwave pulse with duration of 450 ns (Fig. S5 [19]). Therefore, it is expected that the enhancement of TA excitation efficiency should be 86 times. The comparison of conversion efficiency produced by USMP with that generated by the 450 ns pulse is presented in Fig. 3(c). According to the numerical simulation, an improvement of 106 times could be obtained. The experimental result gives an excellent agreement with the theoretical predictions. The deviation between the results may be caused by the jitter of the microwave generator.

The cross sections of two copper wires were imaged to investigate the spatial resolution of the USMP-induced TA imaging. The characteristic diameter of the wire is 130 μm and the distance between them is 450 μm (Fig. S6 [19]).

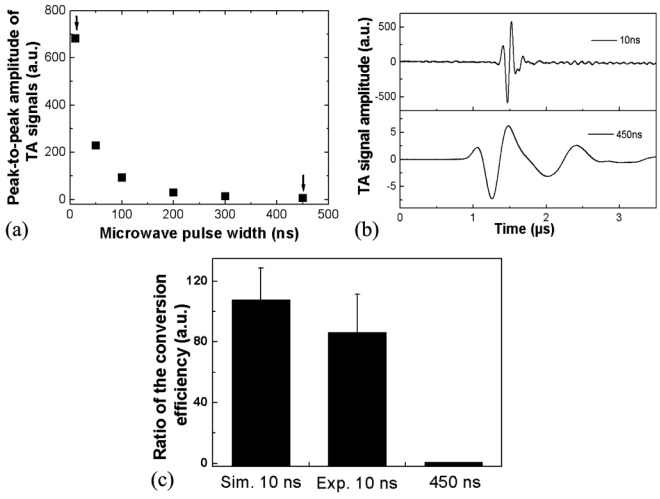

FIG. 3. (a) Amplitude of simulated TA signals that show in Fig. 1(a). (b) TA signals excited by the 450 and 10 ns microwave pulses. (c) The ratio of acoustic-excitation efficiency between USMP-induced and the existing TA.

In the reconstruction image shown in Fig. 4(a), the two wires can be clearly detected. Figure 4(b) plots the normalized intensity profile of cross-section image at $y = 1.84$ mm. The 40.5% amplitude line intercepts the profile at points A, B, C, and D, and it also intercepts the respective centerlines of the two absorption peaks at points E and F. The spatial resolution is estimated according to the Rayleigh criterion. The two sources can no longer be clearly distinguished when point B touches point C in Fig. 4(b). Therefore, the minimum distinguishable distance, R, between the two sources is approximately $R = |EB| + |CF| - 2r$, where r is the radius of the target measured to be 65 μm; hence, the spatial resolution is determined to be 105 μm.

The USMP-induced TA imaging has achieved a spatial resolution of 105 μm, 1 and 2 orders higher than that of the existing TA imaging [1,2,15] and microwave imaging [23], respectively. In the current design, the pulse duration of the microwave is approximately 10 ns, which allows a maximum spatial resolution to be 15 μm. It has been proven that the TA signal is the convolution of the microwave pulse and TA response from a delta function excitation pulse. The USMP was successfully demonstrated as a means of overcoming the resolution limits dictated by the exciting pulse duration.

To demonstrate that the present method could be used to obtain high resolution two-dimensional images, experiments with various microwave pulse excitations were performed, and the reconstructed TA images are illustrated in Fig. 5. The target was a circular-shaped phantom with a diameter of 15 mm. It could be observed that the shorter pulse duration [Fig. 5(b), 10 ns] resulted in a significantly improved resolution and clearer boundary of the target, compared to that with a 450 ns microwave pulse [Fig. 5(a)]. The signal intensity profiles along the marked lines A and B are shown in Fig. 5(c). Quantitatively analyzed, the averaged half-maximum widths of the target boundary in Fig. 5(a) and 5(b) are 1.99 and 0.315 mm, respectively, indicating a 6.3 times improvement in boundary sharpness. Copper wire targets ($d = 300$ or $d = 130$ μm, respectively) with different shapes were further imaged with the USMP-induced TA imaging system to test the imaging ability. Figures 5(d) and 5(e) present the reconstructed TA images and the photographic images are shown as the insets. Both targets can be imaged clearly with excellent contrast, indicating that the USMP-induced TA imaging system can obtain high-imaging resolution.

Compared to that of our previously reported TA imaging system, the implication of the USMP resulted in an increase in the conversion efficiency by 2 orders of magnitude. This significantly reduces the possibility of thermal damage caused by the microwave energy deposition [24], due to the low energy density that is needed for TA excitation. The maximum energy density per pulse employed in this study was ~300 μJ/cm^2, well within the American National Standards Institute's limits [24]. As shown in Fig. 3(b), TA signals from the phantom can be detected with a signal-to-noise ratio (SNR) of 25.8 dB. If we assume that 3 dB SNR is sufficient for imaging, the energy density threshold for high-contrast TA imaging is calculated to be only 21.8 μJ/cm^2, over 2 orders of magnitude lower than that of the existing TA [2,15,22]. This allows high pulse repetition frequency operation of the microwave source, could imply a significant increase in

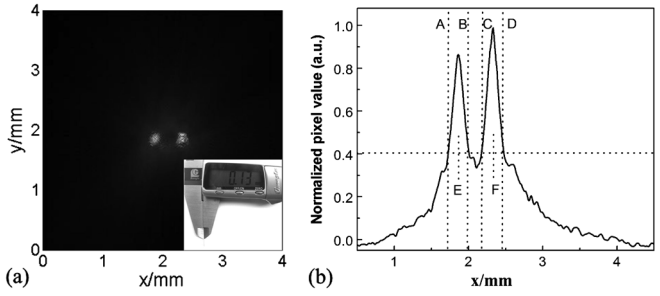

FIG. 4. Spatial resolution of the USMP-induced TA imaging system. (a) TA imaging of two copper wires (0.13 mm in diameter). The inset figure at the bottom-right corner shows the diameter of the wire. (b) Line profile of the reconstructed image shown in (a) with $y = 1.84$ mm.

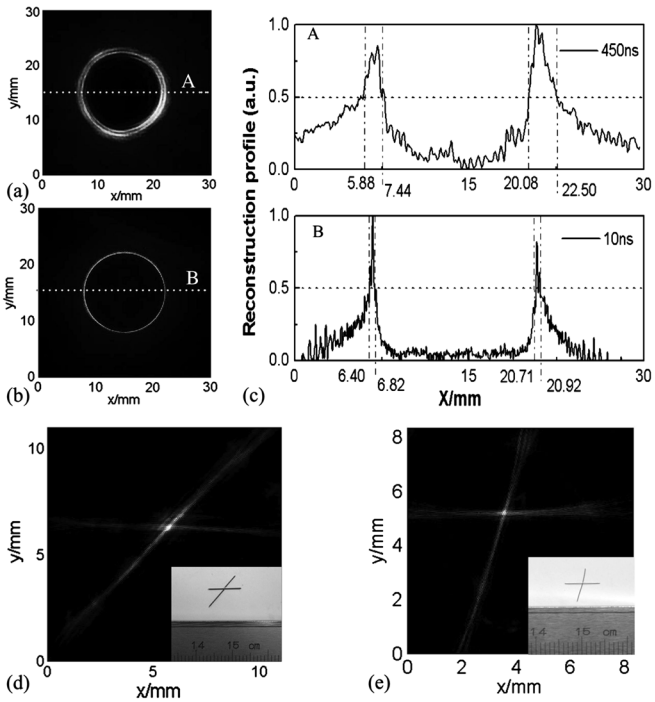

FIG. 5. (a) and (b) Reconstructed TA images of phantom obtained by microwave with a pulse duration of 450 ns and 10 ns, respectively. (c) Signal intensity profiles along the lines A and B marked in (a) and (b). (d) and (e) USMP-induced TA images of copper wire targets with different shapes, $d = 300$ μm for (d), and $d = 130$ μm for (e).

data acquisition for the same imaging period, and points to the use of signal averaging to improve the SNR.

In conclusion, a method based on nanosecond microwave pulse excitation to achieve higher TA excitation efficiency with improved imaging resolution is presented. We have demonstrated that our method has increased the energy conversion efficiency by 2 orders of magnitude. This groundbreaking approach significantly reduces the energy threshold for TA excitation, and shows great potential for noninvasive detection of disease in centimeter depth. USMP induced TA imaging bridges the gap between high-resolution and high-depth imaging and opens up exciting opportunities for noninvasive, high resolution clinical imaging.

We thank Dr. Xuanrong Ji for the technical help and beneficial discussion. This research is supported by the National Basic Research Program of China (2011CB910402, 2010CB732602), the Program for Changjiang Scholars and Innovative Research Team in University (IRT0829), and the National Natural Science Foundation of China (81127004, 11104087).

*Corresponding author.
xingda@scnu.edu.cn

[1] R. A. Kruger, D. R. Reinecke, and G. A. Kruger, Med. Phys. **26**, 1832 (1999).
[2] R. A. Kruger, K. D. Miller, H. E. Reynolds, W. L. Kiser, Jr., D. R. Reinecke, and G. A. Kruger, Radiology **216**, 279 (2000).
[3] M. Xu and L. V. Wang, Med. Phys. **29**, 1661 (2002).
[4] C. H. Li, M. Pramanik, G. Ku, and L. V. Wang, Phys. Rev. E **77**, 031923 (2008).
[5] G. Ku and L. V. Wang, Med. Phys. **28**, 4 (2001).
[6] M. Xu and L. V. Wang, Phys. Rev. E **67**, 056605 (2003).
[7] L. Nie, D. Xing, and S. Yang, Med. Phys. **36**, 3429 (2009).
[8] Y.-S. Chen, W. Frey, S. Kim, P. Kruizinga, K. Homan, and S. Emelianov, Nano Lett. **11**, 348 (2011).
[9] R. R. Letfullin, C. Joenathan, T. F. George, and V. P. Zharov, Nanomedicine **1**, 473 (2006).
[10] L. V. Wang, Nature Photon. **3**, 503 (2009).
[11] D. Razansky, M. Distel, C. Vinegoni, R. Ma, N. Perrimon, R. W. Köster, and V. Ntziachristos, Nature Photon. **3**, 412 (2009).
[12] H. W. Wang, N. Chai, P. Wang, S. Hu, W. Dou, D. Umulis, L. Wang, M. Sturek, R. Lucht, and J.-X. Cheng, Phys. Rev. Lett. **106**, 238106 (2011).
[13] H. F. Zhang, K. Maslov, G. Stoica, and L. V. Wang, Nat. Biotechnol. **24**, 848 (2006).
[14] X. Wang, Y. Xu, M. Xu, S. Yokoo, E. S. Fry, and L. V. Wang, Med. Phys. **29**, 2799 (2002).
[15] L. Nie, D. Xing, Q. Zhou, D. Yang, and H. Guo, Med. Phys. **35**, 4026 (2008).
[16] I. G. Callasso, W. Craig, and G. J. Diebold, Phys. Rev. Lett. **86**, 3550 (2001).
[17] G. J. Diebold, T. Sun, and M. I. Khan, Phys. Rev. Lett. **67**, 3384 (1991).
[18] V. E. Gusev and A. A. Karabutov, *Laser Optoacoustics* (American Institute of Physics, New York, 1993).
[19] See Supplemental Material at http://link.aps.org/supplemental/10.1103/PhysRevLett.109.218101 for methods and supplemental figures.
[20] Y. Zhang, J. Liu, X. Cheng, G. Bai, H. Zhang, J. Feng, and B. Liang, Rev. Sci. Instrum. **81**, 033302 (2010).
[21] J. Liu, Y Zhang, Z. Chen, and J. Feng, IEEE Trans. Electron Devices **57**, 1680 (2010).
[22] L. Nie, D. Xing, D. Yang, L. Zeng, and Q. Zhou, Appl. Phys. Lett. **90**, 174109 (2007).
[23] P. A. Belov, Y. Hao, and S. Sudhakaran, Phys. Rev. B **73**, 033108 (2006).
[24] American National Standard, ANSI Z136.1-2007 77.